Monthly Notices
of the
ROYAL ASTRONOMICAL SOCIETY

MNRAS **454,** 2844–2854 (2015) doi:10.1093/mnras/stv2193

Scaling of the 1-halo terms with bias

L. Raul Abramo,[1]★ Irène Balmès,[1] Fabien Lacasa[2] and Marcos Lima[1]

[1]*Departamento de Física Matemática, Instituto de Física, Universidade de São Paulo, CP 66318, CEP 05314-970 São Paulo, Brazil*
[2]*ICTP South American Institute for Fundamental Research, and Instituto de Física Teórica Universidade Estadual Paulista (UNESP), Rua Dr. Bento Teobaldo Ferraz 271, 01140-070 São Paulo, SP Brazil*

Accepted 2015 September 21. Received 2015 September 21; in original form 2015 June 16

ABSTRACT

In the Halo Model, galaxies are hosted by dark matter haloes, while the haloes themselves are biased tracers of the underlying matter distribution. Measurements of galaxy correlation functions include contributions both from galaxies in different haloes, and from galaxies in the same halo (the so-called one-halo terms). We show that, for highly biased tracers, the one-halo term of the power spectrum obeys a steep scaling relation in terms of bias. We also show that the one-halo term of the trispectrum has a steep scaling with bias. The steepness of these scaling relations is such that the one-halo terms can become key contributions to the n-point correlation functions, even at large scales. We interpret these results through analytical arguments and semi-analytical calculations in terms of the statistical properties of haloes.

Key words: cosmology: theory – large-scale structure of Universe.

1 INTRODUCTION

Galaxy surveys (York et al. 2000; Cole et al. 2005; The Dark Energy Survey Collaboration 2005; Scoville et al. 2007; Adelman-McCarthy et al. 2008b; Tonry et al. 2012; Dawson et al. 2012; Blake et al. 2011; Anderson et al. 2012, 2014) are not just tools for constraining cosmological parameters: they reveal the three-dimensional spatial web of visible structures, the time evolution of these structures, and the history of galaxy evolution. Next-generation surveys are aimed at answering a variety of open astrophysical and cosmological questions, by collecting vast amounts of data at low, intermediate, and high redshifts (Benítez et al. 2009, 2015; LSST Science Collaboration 2009; Schlegel et al. 2009; Ellis et al. 2012; Levi et al. 2013; Dawson et al. 2015).

For the study of how gravity and the Universe's background expansion affect the growth of structure, the standard statistical tools are the n-point correlation functions and their Fourier transforms, the polyspectra. If the distribution of matter were perfectly Gaussian, the two-point correlation function (2pCF) or, equivalently, the matter power spectrum, would contain all the statistical information. However, the primordial fluctuations are believed to be very nearly, but not perfectly, Gaussian. Information about the processes that generated these primordial perturbations is encoded in higher order moments, e.g. the bispectrum (Maldacena 2003). Moreover, when subject to non-linear time evolution, even a perfectly Gaussian initial field develops nontrivial higher order moments (skewness, kurtosis, etc.) whereto statistical information propagates. At late stage of non-linear gravitational evolution, information even leaks out of the hierarchy of moments, as the density field becomes approximately lognormal (Carron 2011, 2012, 2014; Carron & Neyrinck 2012).

Adding to these complications is the fact that we do not directly observe the total matter distribution, but only its visible component – which accounts to ∼20 per cent of the total matter (see e.g. Planck Collaboration XIII 2015) and is affected by non-gravitational effects such as the physics and feedback of baryons, radiation pressure, etc. Hence, the 2pCF of the distribution of visible matter cannot possibly tell the full story and we must treat galaxies, quasars, Ly α systems, etc., as unfaithful (and biased) tracers of the underlying dark matter (DM) distribution.

The relation between tracers of large-scale structure (LSS) and the DM distribution is partially provided by the Halo Model (Cooray & Sheth 2002). The DM haloes – and not the DM particles – then become the fundamental objects. In particular, the correlation functions of the DM haloes are related to the correlation functions of the DM particles by the halo abundance, bias and profile, such that more massive haloes are less abundant, are more highly biased and have less-concentrated profiles.

The statistics of how galaxies populate DM haloes is provided by the so-called Halo Occupation Distribution (HOD; Martinez & Saar 2001; Berlind & Weinberg 2002; Kravtsov et al. 2004; Zheng et al. 2005), which specify how many observable galaxies inhabit a halo as a function of its mass. HOD parameters can be calibrated by measurements of specific abundance ratios, and by fitting the observed correlation functions.

The relationship between the statistics of the halo density field and that of galaxies is often non-trivial. For example, the n-point statistics of galaxies get contributions from the N-halo term (when each galaxy occupies a different halo), from the $(N-1)$-halo term (when two galaxies occupy the same halo, and the others lie in different haloes), etc., all the way down to the one-halo term (when

★E-mail: abramo@fma.if.usp.br

all the N galaxies occupy the same halo). Furthermore, there are contributions to the N-point statistics from $N-1$ types of shot-noise terms: e.g. the $(N-1)$-halo – $(N-1)$-galaxy term (when the correlation function hits twice a galaxy in a given halo, and then only once galaxies in different haloes) down to the one-halo – 1-galaxy term (when the correlation function hits N times the same galaxy). Hence, when we measure the N-point function of galaxies, we are in fact measuring an ad-mixture of all the N'-point functions of haloes ($N' = 1, 2, \ldots, N$).

The galaxy 2pCF includes both a 2-halo term (related to galaxies in two distinct haloes) and a 1-halo term (accounting for galaxies within the same halo). Clearly, the 2-halo term is most important on large scales, within the linear regime, and bears the imprint of the large-scale matter distribution, whereas the 1-halo term dominates on small, non-linear scales, and reflects the matter distribution inside haloes (the halo density profile). Even though these two regimes are connected by time evolution, we may describe the galaxy power spectrum as the superposition of two independent scaling laws: that of the linear DM power spectrum, which dominates on large scales, and that coming from the halo profiles, which dominates on small scales ($k \gtrsim 1\,h\,\mathrm{Mpc}^{-1}$).

In the large-scale limit, the 1-halo term contributes a constant to the galaxy power spectrum. This constant may be poorly known, since galaxy surveys designed for cosmological studies are often insufficiently complete (or have poor redshift accuracy, in the case of photometric redshifts) to determine precisely the HOD parameters for a type of galaxy, and for the survey's mean redshift. This constant represents a noise that must be subtracted from the power spectrum – just as it happens with shot noise, which has a completely different origin but is also a constant that must be subtracted. This feature of the 1-halo term on large scales also comes into play in higher order statistics: the bispectrum gets a constant contribution from the 1-halo term of the 3-point function; the trispectrum gets a constant contribution from the 1-halo term of the 4-point function; and so on.

In this paper, we study the behaviour of the 1-halo terms as a function of the galaxy bias, where these quantities are connected via their mutual dependence on HOD parameters. The same goes for the other observable quantities, such as the mean number density of galaxies, the 2-halo term of the power spectrum, etc. Hence, the HOD provides an internal (but unobservable) parameter space that we can use to vary the observable quantities. In particular, we use the galaxy bias to parametrize the 1-halo terms both because it is more readily available in observations, and also because we are interested in identifying universal behaviours, regardless of the details of the HODs.

We show that, for highly biased tracers ($b_\mathrm{g} \gtrsim 3$), the 1-halo term of the 2pCF obeys a scaling relation in terms of bias, growing as $P^{1h} \sim b_\mathrm{g}^{4-5}$, which is much faster than the scaling of the 2-halo term ($P^{2h} = b_\mathrm{g}^2 P_\mathrm{m}$, where P_m is the matter power spectrum). For highly biased galaxies, the effective shot noise contributed by the 1-halo term can become at least comparable to the Poisson shot noise, significantly lowering the signal-to-noise ratio for measurements of the power spectrum, baryon acoustic oscillations, etc. In some cases, the 1-halo term can even surpass by a large factor the shot noise, as is the case, e.g. for the angular power spectrum of the cosmic infrared background on the angular scales probed by *Herschel* (Thacker et al. 2013). Furthermore, we show that the 1-halo term for the trispectrum also grows very fast – typically, like $(P^{1h})^3$ – and should, therefore, contribute an important source of noise for the power spectrum covariance in the limit of high bias.

When employing a particular cosmological model below, we used a standard flat ΛCDM scenario, with $\Omega_\mathrm{m} = 0.26$, $n_\mathrm{s} = 0.96$, and $\sigma_8 = 0.78$.

2 FORMALISM AND ANALYTICAL APPROXIMATIONS

2.1 The Halo Model

Over time, gravity enhances the density contrast field by attracting matter towards the density peaks, and by creating voids where the density was initially below average. The Halo Model (Cooray & Sheth 2002) describes how this process depends on the mass of the collapsed structures by determining, e.g. the abundances of the DM haloes – i.e. the mass function, $\mathrm{d}\,\bar{n}_h/\mathrm{d}\,\log M$.

Haloes are ultimately determined by the peaks of the initial density field, and according to the theory of peak statistics (Bardeen et al. 1986; Mo & White 1996), the main driver of the abundance of peaks as a function of mass is the mass variance within a certain comoving radius R. The variance of the linear density field inside a spherical top-hat region of radius R is determined by

$$\sigma^2(R) = \frac{1}{2\pi^2}\int \mathrm{d}k\, k^2 P_\mathrm{m}(k) W(kR) = \int \mathrm{d}\ln k\, \Delta^2_\mathrm{m}(k) W(kR), \quad (1)$$

where $P_\mathrm{m}(k)$ is the linear matter power spectrum and $W(x) = [3j_1(x)/x]^2$ is the window function for a spherical top-hat region. The mass contained within radius R at the mean background matter density today, $\bar{\rho}_\mathrm{m}$, is $M(R) = 4\pi R^3 \bar{\rho}_\mathrm{m}/3$. The peak height is defined as $\nu(M) = \delta_\mathrm{c}/\sigma(M)$, where δ_c is the linearly extrapolated critical density contrast for spherical collapse.

Due to the statistics of density peaks (Bardeen et al. 1986), all mass functions exhibit an exponential dependence on the peak height $\nu(M)$. In fact, we have

$$\frac{\mathrm{d}\bar{n}_h}{\mathrm{d}\ln M} = \frac{\bar{\rho}_\mathrm{m}}{M}\frac{\mathrm{d}\ln\sigma^{-1}}{\mathrm{d}\ln M} f(\nu), \quad (2)$$

where, up to some model-dependent factors and coefficients, $f(\nu) \sim e^{-\nu^2/2}$.

Another crucial ingredient of the Halo Model is the halo bias. Since we would like to substitute the true matter density contrast δ_m by the contrast of halo counts, $\delta_\mathrm{h} = n_\mathrm{h}/\bar{n}_\mathrm{h} - 1$, a relationship between the two must be established. We can write this in terms of a local ansatz such as (Fry & Gaztañaga 1993):

$$\delta_\mathrm{h} = b_\mathrm{h}\delta_\mathrm{m} + b_\mathrm{h}^{(2)}(\delta_\mathrm{m}^2 - \sigma_\mathrm{m}^2) + \cdots. \quad (3)$$

In this paper, we will only consider the first term in this relation – the higher order terms can also become important precisely in the limit that we are investigating (tracers with high bias), but we leave this key issue for future investigations. Typically, the halo bias is a smooth power-law function of peak height, such that more massive haloes correspond to higher (and rarer) peaks and have higher values of the halo bias.

Our analytical calculations were performed using both the Press–Schechter (Press & Schechter 1974) (PS) as well as the Sheth–Tormen (Sheth & Tormen 1999; Sheth, Mo & Tormen 1999, ST) prescriptions for the mass function and halo bias. The semi-analytical calculations of Section 3.3 were performed using the Tinker mass function (Tinker et al. 2008) and halo bias (Tinker et al. 2010). The main results are very similar on all cases.

2.2 Halo profile

Related to the Halo Model, but still a slightly orthogonal result which depends more strongly on the non-linear regime of structure formation, is the shape of the halo density profile. Although our results are completely insensitive to the fine details of these profiles, in our semi-analytical calculations we employ the standard results of Navarro, Frenk & White (1997). In that case, the density profile for a halo of mass M is given by

$$\rho(r|M) \sim u(r|M) \sim \frac{1}{\frac{r}{r_s}\left(1+\frac{r}{r_s}\right)^2}, \tag{4}$$

where $r_s = r_s(M)$ is the characteristic scale ('knee') for a halo of mass M. The mass-averaged halo profile in Fourier space is computed as

$$u(k|M) = \frac{4\pi}{M}\int \mathrm{d}r\, r^2\, \frac{\sin kr}{kr}\, \rho(r|M). \tag{5}$$

The important feature for our purpose is that $u(k|M) \to 1$ when $k \lesssim 1\,h$ Mpc^{-1} for the range of masses that we are interested in. This property follows simply from the fact that $u(k \to 0) = (1/M)\int \mathrm{d}^3x\, \rho = 1$, and in the range $k \lesssim 1\,h$ Mpc^{-1} this approximation holds for the mass scales we are interested in. Hence, our calculations are insensitive to the precise adopted profile, and importantly to whether or not the galaxy count profile is identical to the DM density profile. Note indeed that a discrepancy between these two profiles may have been observed in the innermost regions of the DM haloes, where the galaxy profiles may be significantly steeper than the NFW profile (Watson et al. 2010; Kayo & Oguri 2012; Piscionere et al. 2014).

2.3 Halo occupation distribution

It has been known for a long time that there must be a direct relation between the distribution of galaxies and that of the underlying DM haloes (White & Frenk 1991; Kauffmann, White & Guideroni 1993; Navarro, Frenk & White 1995; Mo & White 1996; Kauffmann et al. 1999; Springel et al. 2005). HOD models provide the probability distribution function $P(N|M)$ for a certain number (N) of galaxies to occupy haloes of a given mass (M; Ma & Fry 2000; Seljak 2000; Cooray & Sheth 2002; Martinez & Saar 2001; Berlind & Weinberg 2002; Zheng et al. 2005). Although halo mass is not the only factor which determines the number of galaxies (Zentner, Hearin & van den Bosch 2014), HODs have been extremely useful to interpret measurements of the clustering of different types of tracers, from galaxies (Zheng, Coil & Zehavi 2007; Zheng et al. 2009) to quasars (Porciani, Magliocchetti & Norberg 2004; Shen et al. 2007, 2010; Wake et al. 2008; Kayo & Oguri 2012; Richardson et al. 2012) – however, in the latter case the simplest HODs may be inadequate to capture the complex interactions between quasars and their environments (Chatterjee et al. 2013; Shen et al. 2013; Cen & Safarzadeh 2015), and additional parameters such as assembly bias should be included. Often, instead of $P(N|M)$, what is provided are the momenta of the HOD, such as $\bar{N}(M) = \langle N\rangle_M$, $\langle N(N-1)\rangle_M$, etc. The brackets define averages over haloes of the same mass, and the HOD can be defined in terms of these momenta. For brevity, we will drop the subscript M from now on.

It is clear that, for very massive haloes, the number of galaxies should scale proportionally to the halo mass, but as we approach the low-mass end the situation can be more nuanced. According to the hierarchical scenario of structure formation, a galaxy can either form inside its original halo, or join after formation an already existing and populated halo. Such a dichotomy is also seen in numerical simulations (Kravtsov et al. 2004) and leads to the distinction between 'central' galaxies, of which there can be only one per halo, and possibly numerous 'satellite' galaxies. A popular functional form for the number of central and satellite galaxies is (see e.g. Zheng et al. (2005))

$$\langle N_c\rangle = \bar{N}_c = \frac{1}{2}\,\mathrm{Erfc}\left(\frac{M_c - M}{\sqrt{2}\,\sigma_g}\right) \tag{6}$$

$$\langle N_s\rangle = \bar{N}_s = \bar{N}_c \times \tilde{N}_s, \tag{7}$$

where

$$\tilde{N}_s = \theta(M - \kappa_g M_c)\left(\frac{M - \kappa_g M_c}{M_1}\right)^{\alpha}. \tag{8}$$

As denoted by equation (7), the existence of satellites is conditional on the existence of a central galaxy. Typical values for the HOD parameters are $M_c \simeq 10^{13.5}\,h^{-1}\,\mathrm{M}_\odot$, $M_1 \simeq 10^{14}\,h^{-1}\,\mathrm{M}_\odot$, $\alpha \simeq 0.9$–1.0, $\kappa_g \simeq 1.1$, $\sigma_g \simeq 1$ (Zheng et al. 2005) – although, in the case of quasars, especially at high redshifts, some parameters can deviate significantly from these values (Chatterjee et al. 2013).

Besides the mean numbers (or richness), we must also specify the higher order momenta of $P(N, M)$. If we are only interested in the 2-halo and in the 1-halo terms, then all we need are the expectation values $\langle N_c^2\rangle$, $\langle N_c N_s\rangle$ and $\langle N_s^2\rangle$. The model separating central and satellite galaxies naturally provides these momenta. By definition, the central galaxy either exists ($N_c = 1$) or does not exist ($N_c = 0$) inside a halo so $\langle N_c(N_c - 1)\rangle = 0$ or equivalently $\langle N_c^2\rangle = \bar{N}_c$. Regarding the cross-correlation between central satellite galaxies, notice that satellites can only exist if there is already at least one central galaxy, so $\langle N_c N_s\rangle = \bar{N}_s$. As for the satellites, we can assume a simple Poisson distribution, which means, in particular, that $\langle N_s^2\rangle = \bar{N}_s(\bar{N}_s + 1)$.

2.4 Combining the halo model and the HOD

The Halo Model allows us to compute several quantities of interest from these ingredients. The mean galaxy number density is

$$\bar{n}_g = \int \mathrm{d}\ln M\, \frac{\mathrm{d}\bar{n}_h}{\mathrm{d}\ln M} \times \bar{N}(M), \tag{9}$$

where $\bar{N} = \bar{N}_c + \bar{N}_s$. The galaxy bias is given by

$$b_g(k) = \frac{1}{\bar{n}_g}\int \mathrm{d}\ln M\, \frac{\mathrm{d}\bar{n}_h}{\mathrm{d}\ln M} \times \bar{N}(M) b(M) u(k|M), \tag{10}$$

where recall that $u(k|M) \to 1$ for $k \lesssim 1\,h$ Mpc^{-1}. In terms of the galaxy bias, the two-halo galaxy power spectrum is given by

$$P^{2h}(k) = b_g^2(k) P_m(k). \tag{11}$$

The 1-halo term, on the other hand, is given by the correlation of two *different* galaxies in the *same* halo:

$$\begin{aligned} P^{1h}(k) &= \frac{1}{\bar{n}_g^2}\int \mathrm{d}\ln M\, \frac{\mathrm{d}\bar{n}_h}{\mathrm{d}\ln M} \times \langle N(N-1)\rangle\ |u(k|M)|^2 \\ &= \frac{1}{\bar{n}_g^2}\int \mathrm{d}\ln M\, \frac{\mathrm{d}\bar{n}_h}{\mathrm{d}\ln M} \\ &\quad \times \bar{N}_c(M)\,[2\tilde{N}_s(M) + \tilde{N}_s^2(M)]\ |u(k|M)|^2\,, \end{aligned} \tag{12}$$

where the term inside square brackets in the third line is the intrahalo number variance, given the assumptions outlined above. As usual, the 1-halo term of the power spectrum does not include the contribution arising from self-correlations of galaxies with themselves

(i.e. shot noise): in fact, when there is a single galaxy in a halo, that is, by definition, the central galaxy, so the number of satellites is zero.[1] The measured galaxy power spectrum is therefore

$$P_{\rm g} = P^{2h} + P^{1h} + P_{\rm S}, \tag{13}$$

where $P_{\rm S}$ takes into account the shot noise power spectrum – which, under the assumption of Poissonian statistics for the galaxy counts, is given by $P_{\rm S} = 1/\bar{n}_{\rm g}$.

Similar arguments can also be applied to higher order correlations. The trispectrum $T(\boldsymbol{k}_1, \boldsymbol{k}_2, \boldsymbol{k}_3, \boldsymbol{k}_4)$, i.e. the 4-point function in Fourier space, is of particular interest as it determines the covariance of the power spectrum, in its limit $T(\boldsymbol{k}, -\boldsymbol{k}, \boldsymbol{k}', -\boldsymbol{k}')$. The 1-halo term of this part of the trispectrum is given by

$$\begin{aligned} T_{\rm g}^{\rm 1h}(\boldsymbol{k}, -\boldsymbol{k}, \boldsymbol{k}', -\boldsymbol{k}') &= \frac{1}{\bar{n}_{\rm g}^4} \int {\rm d}\ln M \frac{{\rm d}\bar{n}_{\rm h}}{{\rm d}\ln M} \\ &\quad \times \langle N(N-1)(N-2)(N-3)\rangle \\ &\quad \times |u(k|M)|^2 \left|u(k'|M)\right|^2 \\ &= \frac{1}{\bar{n}_{\rm g}^4} \int {\rm d}\ln M \frac{{\rm d}\bar{n}_{\rm h}}{{\rm d}\ln M} \\ &\quad \times \tilde{N}_{\rm c}[4\tilde{N}_{\rm s}^3 + \tilde{N}_{\rm s}^4] \\ &\quad \times |u(k|M)|^2 \left|u(k'|M)\right|^2, \end{aligned} \tag{14}$$

where on the second line of the equation above we used the same assumptions about the statistics of central and satellite galaxies that were used to obtain the expression in the second line of equation (12).

For our purposes, we will consider scales larger than the size of the largest haloes, so we take $u(k|M) \to 1$ in all our expressions from now on. We have checked that this is an excellent approximation for $k \lesssim 1\,h\,{\rm Mpc}^{-1}$.

2.5 Analytical model for the peak height

In some of the following subsections, we will perform analytical computations of several quantities of interest in the PS (Press & Schechter 1974) and ST (Sheth & Tormen 1999; Sheth et al. 1999) formalisms. In order to carry out those calculations we need an analytical approximation for the peak height in terms of the halo mass.

The variance of the linear density field inside a top-hat spherical region of radius R was given in equation (1). Since the spherical top-hat window function has the features that $W(0) = 1$ and $W \to 0$ for $x \gg 1$, with a full width at half-maximum (FWHM) of approximately $x_{\rm FWHM} \approx 1$, it is fair to approximate the variance as

$$\sigma^2(R) \approx \Delta^2_{\rm m}(k = k_R) \propto k_R^3\, P_{\rm m}(k_R), \tag{15}$$

where $k_R = 1/R$. For self-similar models in which $P_{\rm m}(k) \propto k^n$, we have $\sigma^2(R) \propto k_R^{n+3} \propto R^{-(n+3)}$. In terms of the mass contained inside radius R at the mean background density, $M \propto R^3$, we have

$$\sigma^2(M) \propto M^{-(n+3)/3}. \tag{16}$$

Even though LSS in a standard ΛCDM Universe is not described by a self-similar model, it will be useful to consider this case as it will allow us to obtain interesting analytical expressions for fixed n.

[1] Notice that the one-halo terms vanish in the absence of satellite galaxies. However, due to the Poissonian nature of the HOD, it is possible for a halo to have satellites even if $\langle N\rangle = 1$ for the mass of that halo.

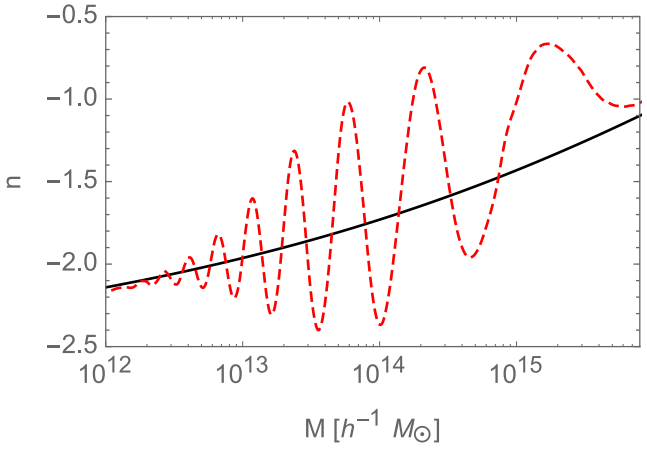

Figure 1. Power-law index as a function of M. Solid (black) line: $n = -3(1 + {\rm d}\ln\sigma^2/{\rm d}\ln M)$. Dashed (red) line: $n_P = {\rm d}\ln P(k)/{\rm d}\ln k$, evaluated at $k = k_R = 1/R(M)$. The wiggles seen in n_P are caused by the BAOs.

The peak height, normalized to 1 at $M = M^*$, is given by

$$\nu = (M/M_*)^{(n+3)/6}, \tag{17}$$

where M_* is typically $\sim 2 \times 10^{13}\,h^{-1}\,{\rm M}_\odot$ in the ΛCDM models. In particular, within this approximation we have ${\rm d}\ln\sigma^{-1}/{\rm d}\ln M = (n+3)/6$.

We check the approximation of equation (16) in Fig. 1, where we plot the power-law index $n = -3(1 + {\rm d}\ln\sigma^2/{\rm d}\ln M)$ (solid, black line) together with $n_P = {\rm d}\ln P(k)/{\rm d}\ln k$, evaluated at $k = k_R = 1/R(M)$ (dashed, red line). The slope of the power spectrum, n_P, shows the wiggles from the BAOs. The power index of the peak height, on the other hand, is an average over several different scales, hence it is only sensitive to the mean slope of the power spectrum. It is clear that the two are closely related, and that the approximation of equation (17) holds quite well for n between -2 and -1 in the mass range considered. In Sections 3.3 and 3.4, we do not use this approximation anymore, and instead compute $\sigma(M)$ from the power spectrum in a ΛCDM model.

2.6 Mass functions and halo bias

The simplest case is that of the PS formalism (Press & Schechter 1974). It provides closed-form expressions for the mass function and halo bias:

$$f_{\rm PS}(\nu) = \sqrt{\frac{2}{\pi}}\,\nu \exp\left[-\nu^2/2\right], \tag{18}$$

$$b_{\rm PS}(\nu) = 1 + \frac{\nu^2 - 1}{\delta_{\rm c}}. \tag{19}$$

These formulas are in poor agreement with the data and N-body simulations, however, when used in conjunction with an extremely simple HOD, they yield simple, straightforward analytical calculations whose results convey the basic message of this paper – see Section 3.1.

A better fit to simulations and observations is given by the ST mass function and halo bias (Sheth & Tormen 1999; Sheth et al.

1999):

$$f_{\rm ST} = A\sqrt{\frac{2a}{\pi}}\left[1+(a\nu^2)^{-p}\right]\,\nu\,e^{-a\nu^2/2}, \tag{20}$$

$$b_{\rm ST} = 1+\frac{a\nu^2-1}{\delta_{\rm c}}+\frac{2p}{\delta_{\rm c}[1+(a\nu^2)^p]}, \tag{21}$$

where $A\simeq 0.322$, $a\simeq 0.71$, and $p\simeq 0.3$. The ST framework gives a more accurate description compared to PS, while still allowing for fully analytical calculations. In Section 3.2, we use the ST formulas and a slightly more realistic HOD compared with the calculation in the PS case – yet the main results of that section are basically unchanged.

Finally, we also consider the expressions found by Tinker et al. (2008, 2010), which were calibrated from numerical simulations. The mass function (Tinker et al. 2008) and bias (Tinker et al. 2010) are given in this case by

$$f(\sigma) = 0.186\times\left[\left(\frac{\sigma}{2.57}\right)^{-1.47}+e^{-1.2/\sigma^2}\right], \tag{22}$$

$$b_{\rm h}(\nu) = 1-A_T\frac{\nu^{a_T}}{\nu^{a_T}+\delta_{\rm c}^{a_T}}+B_T\nu^{b_T}+C_T\nu^{c_T}, \tag{23}$$

where $A_T = 1+0.24\,y\exp[-(4/y)^4]$ (with $y=\log_{10}\Delta$, where we choose $\Delta=200$), $a_T = 0.44\,y-0.88$, $B_T=0.183$, $b_T=1.5$, $C_T = 0.019+0.107\,y+0.19\exp[-(4/y)^4]$, and $c_T=2.4$. We will employ this mass function in our semi-analytical calculations, assuming now a realistic HOD – see Section 3.3. As we shall see shortly, the results are qualitatively identical to those of Sections 3.1 and 3.2, which were found by means of analytical calculations.

3 APPLICATIONS

3.1 PS mass function and a simple HOD

We begin assuming an extremely simplified HOD, which should hold in an approximate sense for sufficiently high halo masses (see e.g. Porciani et al. 2004):

$$\bar{N}(M) = \left(\frac{M}{M_1}\right)^{\alpha}\theta(M-M_1), \tag{24}$$

where $\theta(x)$ is the Heaviside step-function. In this simple HOD, we take the cut-off mass to be equal to the mass scale M_1. This HOD also assumes that all galaxies are satellites. In the final subsections, we recover the full description in terms of $\bar{N}_{\rm c}$ and $\bar{N}_{\rm s}$, and show that the central galaxies are unimportant in the limit we are interested in ($b_{\rm g}\gtrsim 3$). Except for the low-mass limit, the halo richness should scale roughly proportional to its mass, so $\alpha\approx 1$. We will assume for the moment that M_1 also defines the threshold for finding galaxies in haloes – i.e. $\bar{N}=0$ for $M<M_1$. This approximation will be improved in the next subsection, where we carry out the same calculations as here, but using the ST formalism. As we will see, this does not change significantly our main results.

We start by computing the number density of haloes which host at least one galaxy in our simple HOD, equation (24). Since the number of galaxies in each halo follows a Poisson distribution, this is given by

$$\bar{n}_{h/g} = \int {\rm d}\ln M\,\frac{{\rm d}\bar{n}_{\rm h}}{{\rm d}\ln M}\left[1-\exp(-\bar{N})\right] \tag{25}$$

Another definition, which will become more useful later on, is the number of haloes that *could* contain galaxies:

$$\begin{aligned}\bar{n}_{h,g} &= \int_{M_1}^{\infty}{\rm d}\ln M\,\frac{{\rm d}\bar{n}_{\rm h}}{{\rm d}\ln M}\\ &= \int_{M_1}^{\infty}{\rm d}\ln M\,\frac{\rho_{\rm m}}{M}\frac{{\rm d}\ln\sigma^{-1}}{{\rm d}\ln M}\sqrt{\frac{2}{\pi}}\nu\exp[-\nu^2/2]\\ &= \sqrt{\frac{2}{\pi}}\frac{\rho_{\rm m}}{M_*}\int_{\nu_1}^{\infty}{\rm d}\nu\,\nu^{-6/(n+3)}e^{-\nu^2/2},\end{aligned} \tag{26}$$

where we have used the PS mass function and the approximations $M=M_*\nu^{6/(n+3)}$, as well as the definition $\nu_1=(M_1/M_*)^{(n+3)/6}$.

For high M_1 the integral in equation (25) is dominated by the exponential behaviour of the mass function, and we can replace the $\bar{N}$ in the exponent by the mean number of galaxies in the haloes just above the cut-off mass scale, $\bar{N}(M)\to\bar{N}(M_1)=\bar{N}_{\rm min}$. Hence, the actual number of haloes containing galaxies can be approximated by $\bar{n}_{h/g}\approx(1-e^{-\bar{N}_{\rm min}})\times\bar{n}_{\rm h,g}$. For the HOD of equation (24) this minimum mean number of galaxies is $\bar{N}_{\rm min}=1$, so $\bar{n}_{h/g}\approx 0.63\,\bar{n}_{\rm h,g}$.

With the variable change $x\equiv\nu^2/2$ we obtain

$$\bar{n}_{\rm h,g} = \sqrt{\frac{2}{\pi}}\frac{\rho_{\rm m}}{M_*}2^{\lambda_0}\int_{x_1}^{\infty}{\rm d}x\,x^{\lambda_0}e^{-x} = \sqrt{\frac{2}{\pi}}\frac{\rho_{\rm m}}{M_*}2^{\lambda_0}\Gamma(1+\lambda_0,x_1), \tag{27}$$

where $\lambda_0=-1/2-3/(n+3)$, $x_1=\nu_1^2/2$, and $\Gamma(\kappa,x)$ is the (upper) incomplete Gamma function of order κ. Typically, $-2\lesssim n\lesssim -1$ for haloes at the scales of interest, which means that $-7/2\lesssim\lambda_0\lesssim -2$.

The incomplete Gamma function is related to the simple Gamma function by $\Gamma(\kappa)=\Gamma(\kappa,x=0)$, and has asymptotic limits given by

$$\lim_{x\to 0}\Gamma(\kappa,x)\;\to\;\Gamma(\kappa)-x^{\kappa}\left[\frac{1}{\kappa}-\frac{x}{1+\kappa}+\mathcal{O}(x^2)\right], \tag{28}$$

and

$$\lim_{x\to\infty}\Gamma(\kappa,x)\;\to\;e^{-x}\,x^{\kappa-1}\left[1+\frac{\kappa-1}{x}+\mathcal{O}(x^{-2})\right]. \tag{29}$$

Notice, in particular, that $\lim_{x\to\infty}\Gamma(1+\kappa,x)/\Gamma(\kappa,x)\to 1+x+\mathcal{O}(x^{-1})$. It is also interesting to note that, for $0\lesssim\kappa\lesssim 1$, the asymptotic expression of equation (29) is remarkably accurate down to $x\simeq 1$.

Hence, for the ranges of interest for n, in which λ_0 is negative, the number density of the haloes that host galaxies should diverge in the limit $x_1\to 0$ – i.e. when $M_1\ll M_*$. Indeed, the number of haloes of arbitrarily small masses is arbitrarily large, unless we specify a smoothing scale R_f, in which case it asymptotes to $\bar{n}_{\rm h,g}\propto R_f^{-3}$ (Bardeen et al. 1986).

Similarly as was done above, we can compute analytically the quantities defined in Section 2.4. For the mean number density of galaxies we obtain

$$\begin{aligned}\bar{n}_{\rm g} &= \int_{M_1}^{\infty}{\rm d}\ln M\,\frac{{\rm d}\bar{n}_{\rm h}}{{\rm d}\ln M}\times\bar{N}(M)\\ &= \sqrt{\frac{2}{\pi}}\frac{\rho_{\rm m}}{M_*}\left(\frac{M_*}{M_1}\right)^{\alpha}2^{\lambda_1}\Gamma(1+\lambda_1,x_1),\end{aligned} \tag{30}$$

where we have used the same definitions as above, with the difference that now the index is $\lambda_1=\lambda_0+3\alpha/(n+3)=-1/2+3(\alpha-1)/(n+3)$. Since $\alpha\simeq 1$ and $-2\lesssim n\lesssim -1$, we have $\lambda_1\simeq -1/2$. Notice that for

the case $\alpha = 1$, $\lambda_1 = -1/2$ and in the limit $x_1 \to 0$, we have $\bar{n}_g = \rho_m / M_1 = \rho_m \langle N \rangle / M$

Interestingly, using equation (29) we find that in the high mass limit ($x_1 \to \infty$), $\bar{n}_g = \bar{n}_{h,g}$ – i.e. in that case the number of haloes that could host a galaxy is equal to the mean number of galaxies. This is a consequence of the simple HOD, equation (24), which takes the cut-off mass to be identical to the mass scale M_1. Since the galaxy bias increases with M_1, for high values of this mass the number of haloes above the cut-off is exponentially suppressed, and only the least massive haloes are populated with galaxies. In this case, each halo ends up hosting only one galaxy – or, more accurately, because of Poisson statistics, about 63 per cent of haloes contain only one galaxy, and the rest contain two or more galaxies.

We can calculate the galaxy bias in the same fashion, using the PS halo bias of equation (19):

$$b_g = 1 - \delta_c^{-1} + 2\delta_c^{-1} \frac{\Gamma(2 + \lambda_1, x_1)}{\Gamma(1 + \lambda_1, x_1)}. \quad (31)$$

In the $x_1 \to 0$ limit, we can use the property of the Gamma function $\Gamma(2 + \lambda_1) = (1 + \lambda_1)\Gamma(1 + \lambda_1)$, which leads to $b_g \simeq 1 - \delta_c^{-1} + 2\delta_c^{-1}(1 + \lambda_1)$. We also note that taking $\alpha = 1$ leads to $\lambda_1 = -1/2$ and $b_g = 1$, simply reflecting the halo bias consistency relation. On the other hand, in the limit of very large threshold masses ($x_1 \gg 1$) we obtain $b_g \simeq 1 + \delta_c^{-1} + 2\delta_c^{-1} x_1$. Hence, in order to increase bias, it is sufficient that $x_1 \gg 1$ – however, this is not a necessary condition: one could also fix the cut-off mass scale and decrease n, or increase α.

A similar calculation as the one performed in equation (30) leads to an expression for the 1-halo term of the galaxy power spectrum:

$$P^{1h} = \frac{1}{\bar{n}_g^2} \int d\ln M \, \frac{d\bar{n}_h}{d\ln M} \bar{N}^2$$
$$= \left[\sqrt{\frac{2}{\pi}} \frac{\rho_m}{M_*} 2^{2\lambda_1 - \lambda_2} \right]^{-1} \times \frac{\Gamma(1 + \lambda_2, x_1)}{[\Gamma(1 + \lambda_1, x_1)]^2}, \quad (32)$$

where on the first line the term $\langle N(N-1) \rangle$ reduces to $\bar{N}^2$ since we only have satellite galaxies with a Poisson distribution, and on the second line we have substituted the expression for $\bar{n}_g$ and $\lambda_2 = \lambda_0 + 6\alpha/(n+3)$. Using the expression for the number density of haloes hosting these galaxies, equation (26), we obtain:

$$P^{1h} = \frac{\Gamma(1 + \lambda_0, x_1)\,\Gamma(1 + \lambda_2, x_1)}{[\Gamma(1 + \lambda_1, x_1)]^2} \times \frac{1}{\bar{n}_{h,g}}. \quad (33)$$

Notice that the three indices, λ_0 (that appeared in $\bar{n}_{h,g}$), λ_1 (which appeared in $\bar{n}_g$ and b_g), and λ_2, are related by $\lambda_0 = 2\lambda_1 - \lambda_2$. By substituting the asymptotic expression for $\Gamma(\kappa, z)$ in the limit $z \to \infty$ one can verify that the pre-factor appearing equation (33) is $\Gamma(1 + \lambda_0, x_1)\Gamma(1 + \lambda_1, x_1)/[\Gamma(1 + \lambda_1, x_1)]^2 \simeq 1$. Hence, in the limit of high threshold mass, $P^{1h} \approx 1/\bar{n}_{h,g}$.

In the opposite limit, of low threshold masses, the pre-factor can become quite large – but then so does $\bar{n}_{h,g}$ become large. In general, this case corresponds to tracers with low biases. In that limit, it is convenient to revert to the original expression, equation (32), and write instead:

$$P^{1h} = \frac{2^{\lambda_2 - \lambda_1}}{\bar{n}_g} \left(\frac{M_*}{M_1} \right)^{\alpha} \frac{\Gamma(1 + \lambda_2, x_1)}{\Gamma(1 + \lambda_1, x_1)}$$
$$\simeq \frac{2^{\lambda_2 - \lambda_1}}{\bar{n}_g} \left(\frac{M_*}{M_1} \right)^{\alpha} \frac{\Gamma(1 + \lambda_2)}{\Gamma(1 + \lambda_1)}. \quad (34)$$

Let us suppose that we can change the HOD parameters while maintaining the mean number of galaxies, $\bar{n}_g$, fixed. In the limit of low-mass threshold the bias is $b_g \approx 1 - \delta_c^{-1} + \delta_c^{-1}[1 + 6(\alpha - 1)/(n+3)]$ – i.e. higher values of α and/or lower values of n correspond to higher biases. Since $\lambda_2 = \lambda_1 + 3\alpha/(n+3)$, the ratio of Gamma functions in equation (34) can be regarded as a steep function of bias.

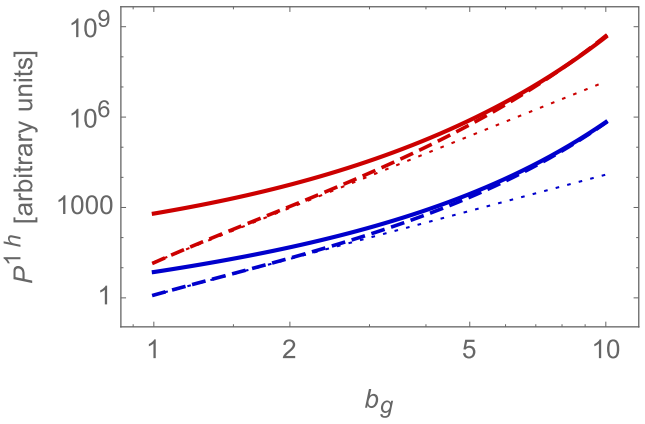

Figure 2. Scaling of the 1-halo term in the PS model. The exact formula, equation (32), is denoted by the thick solid lines (upper line: $n = -2$; lower line: $n = -1$), while the dashed lines correspond to the approximation of equation (36). The dotted lines are the power laws b_g^4 (for the case $n = -1$) and b_g^6 (for the case $n = -2$).

From equation (33) we see that P^{1h}, which is proportional to $1/\bar{n}_{h,g}$, plays the role of a *halo* shot-noise term. For highly biased tracers (whose mass thresholds are relatively high), the galaxies end up in just a few haloes, so that the halo shot noise term becomes an important part of the power spectrum and its covariance. This means, in particular, that the barrier for measuring the (2-halo) power spectrum with highly biased tracers may not be just the shot noise of that tracer, but also an additional *halo shot noise* coming from the 1-halo term.

In the limit of high bias (and high-mass thresholds), we can neglect the subdominant dependence in the pre-factor of $1/\bar{n}_{h,g}$ in equation (33), and express the contribution of the halo shot-noise term as a function of bias. Using $b_g \simeq 1 + \delta_c^{-1} + 2\delta_c^{-1} x_1 \to 2\delta_c^{-1} x_1$, the mean number density of haloes can be expressed as

$$\bar{n}_{h,g} \sim x_1^{-\frac{n+9}{2(n+3)}} e^{-x_1} \sim b_g^{-\frac{n+9}{2(n+3)}} e^{-b_g \delta_c/2}, \quad (35)$$

hence,

$$P^{1h} \sim x_1^{\frac{n+9}{2(n+3)}} e^{x_1} \sim b_g^{\frac{n+9}{2(n+3)}} e^{b_g \delta_c/2}. \quad (36)$$

For intermediate values of the galaxy bias the 1-halo term is well approximated by a power law. In Fig. 2 we show the exact formula, equation (32), for the cases $n = -1$ (lower solid line) and $n = -2$ (upper solid line), in arbitrary units. The first approximation in the middle of equation (36) is plotted as the dashed lines for the two cases, where we used $x_1 \approx (1 - \delta_c + \delta_c b_g)/2$. One can see that the approximation becomes better for higher values of the bias. Also plotted (dotted lines) are the power laws b_g^4 (for the case $n = -1$) and b_g^6 (for the case $n = -2$). The simple power laws shown in Fig. 2 are a good approximation in the interval $1.5 \lesssim b_g \lesssim 3$.

Since the 2-halo term scales as $P^{2h} = b_g^2 P_m$, but the 1-halo term grows much faster with bias, the latter component should become increasingly important for highly biased tracers. In fact, this already happens at small scales ($k \gtrsim 1\,h$ Mpc^{-1}) even for galaxies with relatively low biases. If we select tracers with increasing values of the bias (e.g. quasars), the 1-halo term will become more important,

even in the large-scale limit, acting effectively as a type of 'halo shot noise'. However, in contrast to the usual situation where shot noise can be beaten down by observing a larger number of galaxies, when the tracers are very highly biased this halo shot noise cannot be lowered, and a limiting factor for measuring the power spectrum is the finite number of haloes, and not only the number of galaxies in the survey.

It is easy to see that this argument also applies to higher order correlation functions. The same type of integral computed above appears also in the 1-halo term of the trispectrum, equation (14), and taking $k \to 0$ and $k' \to 0$ leads to:

$$T^{1h} = \frac{1}{\bar{n}_g^4} \int \mathrm{d}\ln M \, \frac{\mathrm{d}\bar{n}_h}{\mathrm{d}\ln M} [4\bar{N}^3 + \bar{N}^4]$$
$$= \frac{1}{\bar{n}_g^4} \times \sqrt{\frac{2}{\pi}} \frac{\rho_m}{M_*} \left[4 \left(\frac{M_*}{M_1} \right)^{3\alpha} 2^{\lambda_3} \Gamma(1+\lambda_3, x_1) + \left(\frac{M_*}{M_1} \right)^{4\alpha} 2^{\lambda_4} \Gamma(1+\lambda_4, x_1) \right], \quad (37)$$

where $\lambda_i = \lambda_0 + i \times 3\alpha/(n+3)$. In the high-mass, high-bias limit we obtain that

$$T^{1h} \sim b_g^{\frac{3}{2}\frac{n+9}{n+3}} e^{3b_g \delta_c/2} \sim \left(P^{1h} \right)^3. \quad (38)$$

Thus T^{1h} will become a dominant part of the power spectrum covariance matrix in the high bias limit.

The same calculation can be employed generally for the 1-halo term of the $N+1$th order polyspectrum in the high bias limit, showing that it grows with the scaling $b_g^{\frac{N}{2}\frac{n+9}{n+3}} e^{N b_g \delta_c/2} \sim \left(P^{1h} \right)^N$.

Hence, we conclude that for highly biased tracers not only the power spectrum, but also the higher-order statistics, are increasingly affected by intrahalo statistics, and may become effectively limited not only by the counts of the tracers, but by the counts of the haloes as well.

3.2 ST mass function and a simple HOD

In this section, we still consider, as before, a simplified HOD which does not distinguish between central and satellite galaxies. However, we now consider a cut-off mass for the halo richness, M_c, which is different from the mass scale M_1 (in fact, typically $M_c < M_1$ – see e.g. Tinker et al. (2008)). Hence, our HOD is

$$\bar{N}(M) = \left(\frac{M}{M_1} \right)^{\alpha} \theta(M - M_c). \quad (39)$$

Defining the variable:

$$x = \frac{a}{2} \nu^2 \to \frac{a}{2} \left(\frac{M}{M_*} \right)^{\frac{n+3}{3}}, \quad (40)$$

and the cut-of

$$x_c = \frac{a}{2} \left(\frac{M_c}{M_*} \right)^{\frac{n+3}{3}}, \quad (41)$$

the calculations of the previous section can now be performed in basically the same fashion. The number density of haloes that can host galaxies is

$$\bar{n}_{h,g} = \frac{\rho_m}{M_*} \frac{A}{\sqrt{\pi}} \left(\frac{2}{a} \right)^{\lambda_0} \int_{x_c}^{\infty} \mathrm{d}x \, x^{\lambda_0} \left[1 + (2x)^{-p} \right] e^{-x}$$
$$= \bar{n}_0 \left(\frac{2}{a} \right)^{\lambda_0} \left[\Gamma(1+\lambda_0, x_c) + 2^{-p} \Gamma(1+\lambda_0 - p, x_c) \right], \quad (42)$$

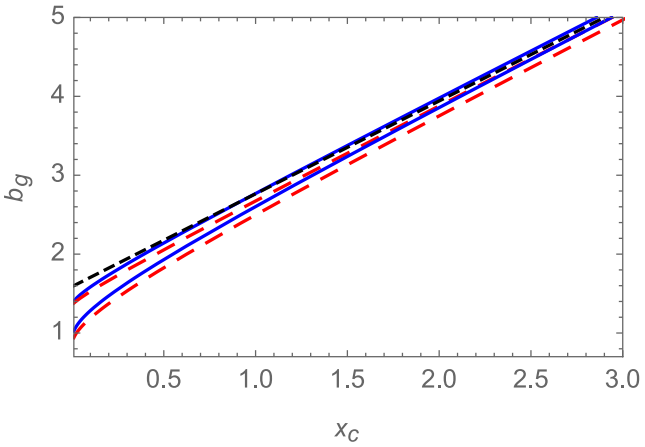

Figure 3. Galaxy bias obtained using the ST formalism (blue lines and filled region), and in the PS formalism (red, long-dashed lines and filled region), as a function of the cut-off scale x_c [see equation (41)]. The parameters were allowed to range in the intervals $0.9 < \alpha < 1.1$, and $-2 < n < -1$. The black (short-dashed) line shows the approximation of equation (45).

where, as previously, $\lambda_0 = -1/2 - 3/(3+n)$, and we have defined $\bar{n}_0 = \rho_m A / M_* \sqrt{\pi}$.

A similar calculation leads to the mean number density of galaxies:

$$\bar{n}_g = \bar{n}_0 \left(\frac{M_*}{M_1} \right)^{\alpha} \left(\frac{2}{a} \right)^{\lambda_1} \times \left[\Gamma(1+\lambda_1, x_c) + 2^{-p} \Gamma(1+\lambda_1 - p, x_c) \right], \quad (43)$$

and the galaxy bias becomes

$$b_g = 1 - \delta_c^{-1} + \frac{2\delta_c^{-1}}{\Gamma(1+\lambda_1, x_c) + 2^{-p}\Gamma(1+\lambda_1 - p, x_c)} \times \left[\Gamma(2+\lambda_1, x_c) + 2^{-p}\Gamma(2+\lambda_1 - p, x_c) + p\, 2^{-p} \Gamma(1+\lambda_1 - p, x_c) \right]. \quad (44)$$

In the limit of $x_c \gg 1$ the galaxy bias can be considerably simplified, in fact

$$\lim_{x_c = \infty} b_g \to 1 - \delta_c^{-1} + 2\delta_c^{-1} x_c, \quad (45)$$

which is basically the approximate expression we obtained in the PS case, where x_1 played the role of the cut-off mass scale. This relationship between the cut-off scale and the bias allows us to write, in the limit of high biases, $x_c \simeq \delta_c (b_g - 1 + \delta_c^{-1})/2$. This turns out to be a fairly good approximation as can be seen from Fig. 3. Notice that we do not expect the model of equation (39) to hold for low-biased galaxies, when the small-halo mass limit is critical.

After some algebra, the 1-halo term can be expressed in the same way as was done for the PS case:

$$P^{1h} = q \, \frac{1}{\bar{n}_{h,g}}, \quad (46)$$

where

$$q = \frac{\Gamma(1+\lambda_0, x_c) + 2^{-p}\Gamma(1+\lambda_0 - p, x_c)}{\left[\Gamma(1+\lambda_1, x_c) + 2^{-p}\Gamma(1+\lambda_1 - p, x_c) \right]^2} \times \left[\Gamma(1+\lambda_2, x_c) + 2^{-p}\Gamma(1+\lambda_2 - p, x_c) \right]. \quad (47)$$

In the limit of $x_c \gg 1$ we can use the series expansion of equation (29) to show that, as in the PS case, the pre-factor $q \to 1$.[2] In this limit P^{1h} reduces to the following expression:

$$P^{1h} \simeq \left[\bar{n}_0 \left(\frac{2}{a}\right)^{\lambda_0} x_c^{\lambda_0} \left(1 + 2^{-p} x_c^{-p}\right) e^{-x_c}\right]^{-1} \quad (48)$$

with x_c depending on the bias in the following way:

$$x_c = \frac{\delta_c}{2}(b_g - 1 + \delta_c^{-1}). \quad (49)$$

Conversely, in the limit $x_c \ll 1$, we obtain the following scaling for the one-halo term:

$$P^{1h} \simeq \frac{\Gamma(1+\lambda_2) + 2^{-p}\Gamma(1+\lambda_2 - p)}{\bar{n}_0 \left(\frac{2}{a}\right)^{\lambda_0} [\Gamma(1+\lambda_1) + 2^{-p}\Gamma(1+\lambda_1 - p)]^2}. \quad (50)$$

Comparing equation (36) and equation (48), we see that, for high values of the bias, the 1-halo term in the ST model behaves in basically the same way as was found for the PS formalism.

3.3 Semi-analytical model: Tinker mass function and realistic HOD

The analytical approximations of the previous sections have allowed us to obtain simple expressions for the number densities of galaxies and haloes, the bias, and the 1-halo terms, but we made some strong assumptions – in particular, about the simple scaling of halo richness, about the assumption of self-similarity which fixed the scaling of ν with mass, and about the way in which we cut off the halo richness below some given mass scale. Although the final results may have seemed natural and physically sensible, they could have been influenced or even driven by these simplifications.

In this section, we argue that these results are robust. We show this by improving the modelling of the previous sections in a number of ways: first, we calculate the mass variance $\sigma(M)$ of equation (1) from the power spectrum of a vanilla-ΛCDM model; secondly, we employ the Tinker et al. (2008) mass function and halo bias of equations (22)–(23), which are a slightly better fit to the N-body simulations compared to the PS or ST expressions; and thirdly, we use a class of HODs which is inspired and calibrated by observations (Zheng et al. 2005, 2007, 2009). We also distinguish between central and satellite galaxies – whereas in the preceding sections we implicitly assumed that all galaxies were satellites.

As for the HOD, we have used the formulas of equations (6)–(7) for the halo richness of central and satellite galaxies. Typical values for these parameters are $M_c \simeq 10^{13.5}\, h^{-1}\,\mathrm{M}_\odot$, $M_1 \simeq 10^{14.}\, h^{-1}\,\mathrm{M}_\odot$, $\alpha \simeq 0.9$, $\kappa_g \simeq 1.1$, and $\sigma_g \simeq 1$ (Zheng et al. 2009).

In contrast to the previous sections, where all calculations could be carried out exactly, here we instead compute numerically the galaxy number density of equation (9), the bias of equation (10), and the 1-halo term of equation (12). In this way we can explore basically any point in parameter space, and compute the properties of the galaxy models corresponding to those points.

[2] In this limit, we see from equation (46) that the 1-halo term of the power spectrum inherits a dependence on the number density of the haloes that contain at least one galaxy. However, the HOD we used in this section and in the previous one make no distinction between central and satellite galaxies – in fact, we have simply used the typical parametrizations used for satellites. Hence, in this context, $\bar{n}_{h,g}$ should be regarded as the number density of haloes containing *more* than one galaxy.

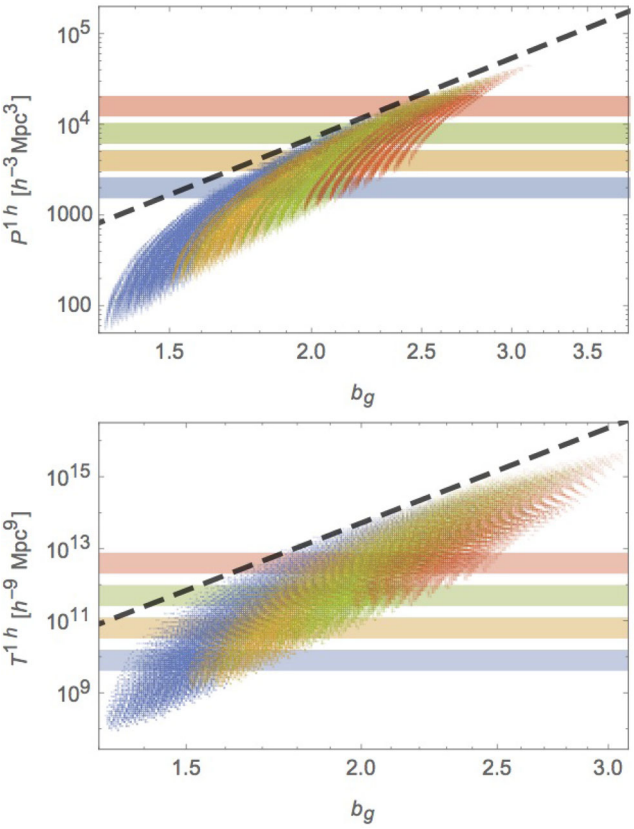

Figure 4. Top panel: 1-halo term in the HOD of equations (6)–(7). The models were split according to the number density of galaxies. From left to right, and from the bottom up, the models shown have $10^{-3.15} \geq \bar{n}_g \geq 10^{-3.45}$, $10^{-3.45} \geq \bar{n}_g \geq 10^{-3.75}$, $10^{-3.75} \geq \bar{n}_g \geq 10^{-4.05}$, and $10^{-4.05} \geq \bar{n}_g \geq 10^{-4.35}$. In each case, the horizontal shaded area marks the corresponding range of $1/\bar{n}_g$. The dashed black line is the power law $b_g^{4.5}$. The stripes seen mostly in the lower-right corner are just an artefact of the grid we used to explore the HOD parameter space. Bottom panel: 1-halo term of the trispectrum for the same class of HODs. The dashed black line is the power law $b_g^{13.5}$. The horizontal shaded areas mark the corresponding ranges of $1/\bar{n}_g^3$.

We allow the parameters to vary in the following ranges, while keeping always $M_c \leq M_1$:

$$12.75 < \log_{10} M_c\, h/\mathrm{M}_\odot < 14.25, \quad (51)$$

$$13.2 < \log_{10} M_1\, h/\mathrm{M}_\odot < 15.0, \quad (52)$$

$$0.85 < \alpha < 1.15, \quad (53)$$

$$0.85 < \sigma_g < 1.15, \quad (54)$$

$$1.0 < \kappa_g < 1.3. \quad (55)$$

The results for the 1-halo term of the power spectrum are shown in the top panel of Fig. 4. We have split the different HOD models in four groups, according to the number densities of galaxies. From the bottom, the horizontal shaded areas correspond to HODs whose ranges of $\bar{n}_g^{-1}$ fall in the intervals $10^{-L+0.15} \geq \bar{n}_g\,(h^3\,\mathrm{Mpc}^{-3}) \geq 10^{-L-0.15}$, for $L = 3.3$, 3.6, 3.9, and 4.2. The values of P^{1h} for models in those four groups are shown as points of the same colours as the shaded areas, from lower-left to upper-right, respectively. The dashed black line is the power law $b_g^{4.5}$.

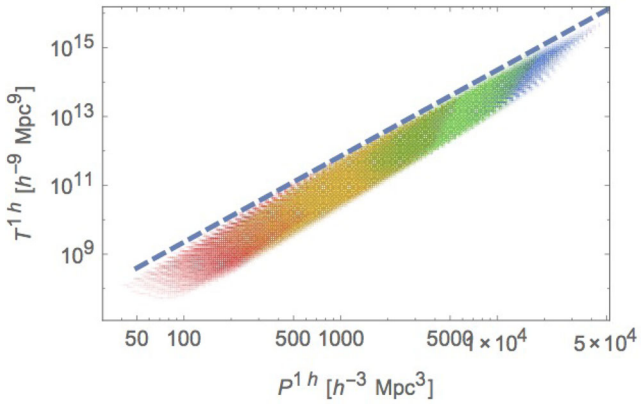

Figure 5. 1-halo term of the trispectrum plotted against the 1-halo term of the power spectrum, for the HOD of equations (6)–(7). The dashed black line is the power law $(P^{1h})^{2.5}$. The models were split according to bias: from lower-left to upper-right, the different colours indicate models with $1.0 \leq b_g \leq 1.5$, $1.5 \leq b_g \leq 2.0$, $2.0 \leq b_g \leq 2.5$, and $2.5 \leq b_g \leq 3.0$.

We saw in Sections 3.1 and 3.2 that the 1-halo term evolves like a power-law in b_g for intermediate values of the galaxy bias. This is again what we observe here: the asymptotic behaviour of the one-halo follows a steep power law as a function of galaxy bias. The growth of the 1-halo term is constrained by the requirement that $M_c \leq M_1$, which limits the number of galaxies in haloes, and imposes an upper limit on the bias and the 1-halo term. If we relax this physical requirement, the power-law evolution of the 1-halo term continues at higher bias.

The results obtained in Sections 3.1 and 3.2 were derived under the assumption that all galaxies are of the 'satellite' type – an approximation that we did not use here. For highly biased tracers the 1-halo term can be comparable to Poisson shot noise, which shows that the 'central' galaxies are less relevant in that limit, providing a motivation for that approximation in Sections 3.1 and 3.2. Conversely, the fact that P^{1h} drops well below the level of galaxy shot noise for low values of the bias shows that, for such types of objects, the central galaxy plays an important role, as many (or most) haloes host a single central galaxy.

In the bottom panel of Fig. 4, we show the results for the 1-halo term of the trispectrum of equation (14), in the limit $k \to 0, k' \to 0$, for the same range of HOD parameters used in the top panel. Again, we separate the models in groups, according to the number density of galaxies, and the horizontal shaded areas denote the different values of n_g^{-3} for each group. The dashed line is the power law $b_g^{13.5}$.

As argued above, the 1-halo term of the trispectrum also scales rapidly with bias, approximately as $(P^{1h})^3$. In Fig. 5, we show the 1-halo term of the trispectrum [equation (14)] against the 1-halo term of the power spectrum. The dashed line indicates the scaling $(P^{1h})^{2.5}$.

3.4 Simulations

We further test the results from the previous sections in a fully numerical setup, by using a catalogue of haloes from the DEUS simulations[3] (Alimi et al. 2010; Rasera et al. 2010; Courtin et al. 2011). We use haloes detected with the Friends-of-Friends algorithm in a box of $648h^{-1}$ Mpc, containing 1024^3 DM particles, in a ΛCDM cosmology in agreement with *WMAP*5 (Komatsu et al. 2009). We should note that the DEUS mass function is very well fit by the Tinker mass function, and that the DEUS halo bias is also well fit by the Tinker halo bias.

We populate the haloes using the HOD formalism presented in equations (6) and (7), with fixed parameters $\alpha = 0.9$, $\sigma_g = 1.0$ and $\kappa_g = 1.1$. The M_c and M_1 parameters are allowed to vary in the ranges given in equations (51)–(52).

The number N_c of central galaxies is either 0 or 1, and is drawn from a nearest-integer uniform distribution with mean $\bar{N}_c$. For haloes containing a central galaxy, the number of satellite galaxies is then drawn from a Poisson distribution with mean $\tilde{N}_s$ (since we are taking the $k \to 0$ limit for the 1-halo term, it is irrelevant where in the halo those satellite galaxies are placed). Obviously, haloes that do not contain a central galaxy have no satellite galaxies.

With the DEUS halo catalogue, and the HOD implementation described above, expressions such as that for the number density of galaxies become:

$$\begin{aligned}\bar{n}_g &= \int_{M_1}^{\infty} \mathrm{d}\ln M \, \frac{\mathrm{d}\bar{n}_h}{\mathrm{d}\ln M} \times \bar{N}(M) \\ &\longrightarrow \frac{1}{V}\sum_h \{N_c[M(h)] + N_s[M(h)]\} \\ &= \frac{1}{V}\sum_M N_h(M)\,[\bar{N}_c(M) + \bar{N}_s(M)], \end{aligned} \tag{56}$$

where V is the volume of the simulation. In order to compute galaxy bias, for simplicity we employ the Tinker bias, equation (23), in equation (10).

The resulting scaling between the 1-halo term and the galaxy bias is shown in the top panel of Fig. 6. The same type of scaling found in the previous sections appears here – the grey line indicates the power law $P^{1h} \propto b_g^5$. In order to check whether this scaling is sensitive to the precise form of the HOD used, we also test a different HOD prescription for which

$$\bar{N}_g \propto \log \frac{M}{M_c} \text{ for } M > M_c. \tag{57}$$

The number of galaxies in each halo is drawn from a Poisson distribution with mean given by the formula above. The scaling obtained in this case between the 1-halo term and the galaxy bias is shown on the bottom panel of Fig. 6. The grey line now follows $b_g^{4.5}$, a scaling very similar to the one found in the previous cases.

As is the case in the original HOD of the previous sections, in this alternative HOD prescription the richness is an increasing function of halo mass. We also tested HOD models where the richness becomes constant, or even decreases, with increasing halo mass, and in those cases we do not recover the same type of scaling between bias and the 1-halo term of the power spectrum. However, we do not consider this to be a limitation of our study, as we expect realistic HODs to display an average number of galaxies monotonically increasing with halo mass.

4 DISCUSSION

We have shown that, when the galaxy bias is high enough ($b_g \gtrsim 3$), the 1-halo term of the power spectrum grows faster as a function of bias than the 2-halo term. We also showed that the 1-halo term of the trispectrum grows much faster than the 4-halo term. We argue that the 1-halo terms of all the N-polyspectra scale faster than the N-halo terms of those polyspectra.

[3] http://www.deus-consortium.org

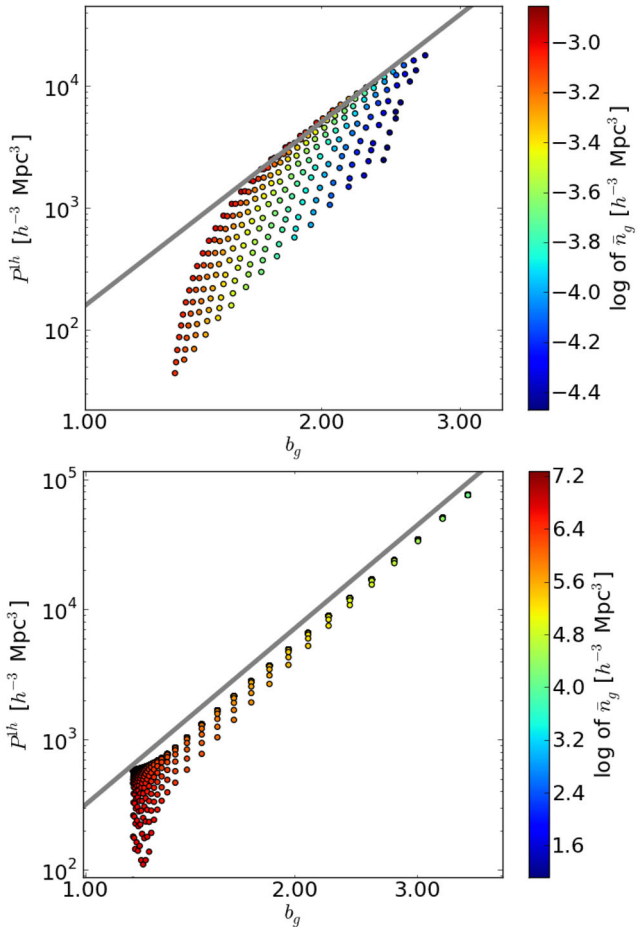

Figure 6. 1-halo term and galaxy bias obtained from the DEUS simulated halo catalogue populated with the HOD of equations (6)–(7) (top panel), and with the test HOD of equation (57) (bottom panel). In the top panel, the grey line shows the scaling b_g^5, while in the bottom panel the scaling is $b_g^{4.5}$.

We interpret these results in the following way. Galaxy bias provides an intuitive physical interpretation of the way in which the visible matter distribution is related to the underlying DM distribution. Given a Gaussian field δ_G, taken from a distribution whose variance (in Fourier space) is basically the matter power spectrum, the density contrast of a biased tracer on a grid of finite-volume cells can be approximated by a lognormal field, $\delta_g = \exp[b_g\delta_G - b_g^2\sigma_G^2/2] - 1$, where b_g is the bias of the tracer, and σ_G^2 is the variance of the Gaussian field on the volume of the cell of the grid (Coles & Jones 1990). As the bias increases, the number of particles found in the density peaks grow very fast (Bardeen et al. 1986) – exponentially, in the lognormal model – while most of the space is emptied.

In terms of the Halo Model, we can vary the HOD parameters in such a way that the mean number density is kept fixed while the bias increases. For highly biased galaxies we expect to find more objects concentrated in fewer haloes. This implies that, for very high values of the bias, the galaxy 2-point statistics can get a large contribution from the statistics of haloes hosting two or more galaxies. This argument extends to all the N-point statistics: in the high-bias limit there will be many galaxies inside the same few haloes, which means that all the 1-halo terms of the N-point statistics will become increasingly important.

In Section 3.1, within the Press & Schechter (1974) formalism, we used very simple formulas for the halo richness and for the scaling of the mass variance (and peak height), to show that the 1-halo term of the power spectrum grows very fast with bias. A more refined analytical calculation, done in Section 3.2 using the Sheth & Tormen (1999) framework, shows basically the same scaling. In Section 3.3, we employed the Tinker et al. (2008) mass function, realistic HODs, and an exact computation of the mass variance in ΛCDM models, and confirmed that the 1-halo term of the power spectrum scales at least as fast as $P^{1h} \sim b_g^{4-5}$. Similarly, we showed that the 1-halo term of the trispectrum scales as fast as $T^{1h} \sim b_g^{12-15}$. Finally, in Section 3.4 we used a halo catalogue derived from the DEUS simulation, and two different kinds of HODs, and again obtained the same scaling laws.

The fact that simple analytical arguments show the correct scaling of the 1-halo terms with bias is a hint that these results should be related to basic properties of Gaussian fields and the matter power spectrum. In fact, tracers of different biases effectively probe different scales in the power spectrum: higher/lower masses (and higher/lower biases) are related to larger/smaller scales. Since the matter power spectrum has a power index that ranges between $n \simeq -1$ at large scales, to $n \simeq -2$ at small scales, the power index which is relevant for the halo masses typical of a certain type of galaxy is also an indicator of the bias of that galaxy. Conversely, bias also tells us how galaxies are distributed among the DM haloes, and about the typical peak height which corresponds to a galaxy with that bias. In particular, a higher bias implies that galaxies will be more concentrated on fewer haloes, enhancing the 1-halo terms. Since all these properties can be traced back to the slope of the power spectrum, it is not surprising to find that different types of galaxies present the same scaling of the 1-halo term with bias.

Since the 1-halo terms are constant on large scales, for cosmological surveys that cannot resolve the inner structure of haloes, these terms enter effectively as additional sources of noise and covariance. Conversely, very accurate and complete surveys will be able to detect much better the amplitudes and scale dependences of the 1-halo terms when the bias is sufficiently high, implying better constraints on HOD parameters.

In particular, cosmological surveys targeting highly biased objects could be severely impacted by the effects of the statistics of counts of the haloes hosting those objects. Measurements of the power spectrum from these surveys should take into account not only the higher effective shot noise coming from the 1-halo term of the power spectrum, but also the additional contribution to the power spectrum covariance coming from the 1-halo term of the trispectrum. Similarly, measurements of the bispectrum which employ highly biased tracers should ensure that the relevant 1-halo terms are properly taken into account.

Finally, although we worked at $z = 0$, it would be interesting to find out what happens at high redshifts. On the one hand, the bias of a given population of tracers is typically increasing as a function of redshift; but on the other hand, linear theory should become a better approximation, which means that the 1-halo term should be less important. Therefore, at higher redshifts the form of the scaling of the 1-halo term should depend sensitively not only on the amplitude of the power spectrum, but also on the evolution of the HOD parameters.

The cosmic infrared background (CIB) is a good example: in that case (redshifts $z \sim 1 - 4$), the 1-halo term has a higher amplitude compared with shot noise, which helped constrain the HOD of the sources the CIB (Thacker et al. 2013). A similar situation may arise as galaxy surveys aim at deeper redshifts and higher number densities with objects such as emission-line galaxies and quasars (e.g. JPAS (Benítez et al. 2015); eBOSS (Dawson et al. 2015); DESI

(Levi et al. 2013); PFS (Ellis et al. 2012)), HI intensity maps (with, e.g. SKA[4]), etc.: the amplitude of the 1-halo terms should be kept in check in order to ensure the reliability of the forecasts from these surveys. We plan to examine in future work how extrapolations of the existing HODs to higher redshifts impact the signal-to-noise levels and the cosmological constraints for some future galaxy surveys.

ACKNOWLEDGEMENTS

We would like to thank Marcello Musso and Ravi Sheth for useful discussions, and Aurélie Pénin for many insightful comments. We acknowledge support from the DIM ACAV of the Region Île-de-France for the storage of the DEUS data. We would also like to thank FAPESP, CAPES, CNPq, and the University of São Paulo's *NAP LabCosmos* for financial support. IB acknowledges support from FAPESP through the grant 2013/21069-9, and FL acknowledges support from FAPESP through grants 2011/11973 and 2013/19936-6.

REFERENCES

Abramo L. R. et al., 2012, MNRAS, 423, 3251-PLX1
Adelman-McCarthy J. K. et al., 2008b, ApJS, 175, 297
Alimi J.-M., Füzfa A., Boucher V, Rasera Y., Courtin J., Corasaniti P. S., 2010, MNRAS, 401, 775
Anderson L. et al., 2012, MNRAS, 427, 3435
Anderson L. et al., 2014, MNRAS, 439, 83
Bardeen J. M., Bond J. R., Kaiser N., Szalay A. S., 1986, ApJ, 304, 15
Benítez N. et al., 2009, ApJ, 691, 241
Benítez N. et al., 2015, in Cenarro A. J., Figueras F., Hernndez-Monteagudo C., Trujillo Bueno J., Valdivielso L., eds, Proc. XI Sci. Meeting Spanish Astron. Soc., Highlights of Spanish Astrophysics VIII. Teruel, Spain, p. 148
Berlind A. A., Weinberg D. H., 2002, ApJ, 575, 587
Blake C. et al., 2011, MNRAS, 415, 2876
Carron J., 2011, ApJ, 738, 86
Carron J., 2012, Phys. Rev. Lett., 108, 7
Carron J., 2014, preprint (arXiv:1406.6095)
Carron J., Neyrinck M. C., 2012, ApJ, 750, 1
Cen R., Safarzadeh M., 2015, ApJ, 798, L38
Chatterjee S., Nguyen M. L., Myers A. D., Zheng Z., 2013, ApJ, 779, 147
Cole S. et al., 2005, MNRAS, 362, 505
Coles P., Jones B., 1990, MNRAS, 248, 1
Cooray A., Sheth R., 2002, Phys. Rep., 372, 1
Courtin J., Rasera Y., Alimi J.-M., Corasaniti P. S., Boucher V., Füzfa A., 2011, MNRAS, 410, 1911
Dalal N., Doré O., Huterer D., Shirokov A., 2008, Phys. Rev. D, 77, 123514
Dawson K. et al., 2012, AJ, 145, 10
Dawson K. et al., 2015, preprint (arXiv:1508.04473)
Ellis R. (The PFS Team) et al., 2012, PASJ, 66, R1
Fry J., Gaztañaga E., 1993, ApJ, 413, 447
Kauffmann G., White S. D. M., Guiderdoni B., 1993, MNRAS, 264, 201
Kauffmann G., Colberg J. M., Diaferio A., White S. D. M., 1999, MNRAS, 303, 188
Kayo I., Oguri M., 2012, MNRAS, 424, 1363
Komatso E. et al., 2009, ApJS, 180, 330
Kravtsov A. V., Berlind A. A., Wechsler R. H., Klypin A. A., Gottlber S., Allgood B., Primack J. R., 2004, ApJ, 609, 35
Levi M. et al., 2013, preprint (arXiv:1308.0847)
Linder E., 2005, Phys. Rev. D, 72, 043529
LSST Science Collaboration, 2009, preprint (arXiv:0912.0201)
Ma C.-P., Fry J. N., 2000, ApJ, 543, 503
Maldacena J., 2003, J. High Energy Phys., 05, 013
Martinez V., Saar E., 2001, Statistics of the Galaxy Distribution. CRC Press, Florida
Mo H., White S. D. M., 1995, MNRAS, 282, 347
Navarro J. F., Frenk C. S., White S. D. M., 1995, MNRAS, 275, 56
Navarro J. F., Frenk C. S., White S. D. M., 1997, ApJ, 490, 483
Piscionere J. A., Berlind A. A., McBride C. K., Scoccimarro R., 2015, ApJ, 806, 125
Planck Collaboration XIII, 2015, preprint (arXiv:1502.01589)
Porciani C., Magliocchetti M., Norberg P., 2004, MNRAS, 355, 1010
Press W. H., Schechter P., 1974, ApJ, 187, 425
Rasera Y., Alimi J.-M., Courtin J., Roy F., Corasaniti P.-S., Füzfa A., Boucher V., 2010, in Alimi J.-M., Füzfa A., eds, AIP Conf. Proc. Vol. 1241, Introducing the Dark Energy Universe Simulation Series (DEUSS). Am. Inst. Phys., New York, p. 1134
Richardson J., Zheng Z., Chatterjee S., Nagai D., Shen Y., 2012, ApJ, 755, 30
Schlegel D. J. et al., 2009, preprint (arXiv:0904.0468)
Scoville N. et al., 2007, ApJS, 172, 1
Seljak U., 2000, MNRAS, 318, 203
Shen Y. et al., 2007, AJ, 133, 2222
Shen Y. et al., 2010, ApJ, 719, 1693
Shen Y. et al., 2013, ApJ, 778, 98
Sheth R. K., Tormen G., 1999, MNRAS, 308, 119
Sheth R. K., Mo H. J., Tormen G., 2001, MNRAS, 323, 1
Springel V. et al., 2005, Nature, 435, 629
Thacker C. et al., 2013, ApJ, 768, 58
The Dark Energy Survey Collaboration, 2005, preprint (astro-ph /0510346)
Tinker J., Kravtsov A. V., Klypin A., Abazajian K., Warren M., Yepes G., Gottlöber S., Holz D. E., 2008, ApJ, 688, 709
Tinker J. L., Robertson B. E., Kravtsov A. V., Klypin A., Warren M. S., Yepes G., Gottlöber S., 2010, ApJ, 724, 878
Tonry J. L. et al., 2012, ApJ, 750, 99
Wake D. A., Croom S. M., Sadler E. M., Johnston H. M., 2008, MNRAS, 391, 1674
Watson D. F., Berlind A. A., McBride C. K., Masjedi M., 2010, ApJ, 709, 115
White S., Frenk C., 1991, ApJ, 379, 52
York D. G. et al., 2000, AJ, 120, 1579
Zentner A. R., Hearin A. P., van den Bosch F. C., 2014, MNRAS, 443, 3044
Zheng Z. et al., 2005, ApJ, 633, 791
Zheng Z., Coil A., Zehavi I., 2007, ApJ, 667, 760
Zheng Z., Zehavi I., Eisenstein D. J., Weinberg D. H., Jing Y. P., 2009, ApJ, 707, 554

[4] http://www.skatelescope.org/

This paper has been typeset from a TEX/LATEX file prepared by the author.